Journal of Molecular Graphics and Modelling 48 (2014) 36–46

Contents lists available at ScienceDirect

Journal of Molecular Graphics and Modelling

journal homepage: www.elsevier.com/locate/JMGM

Insight into the structural mechanism for PKBα allosteric inhibition by molecular dynamics simulations and free energy calculations

Shi-Feng Chen, Yang Cao, Shuang Han, Jian-Zhong Chen*

Institute of Materia Medica, College of Pharmaceutical Sciences, Zijingang Campus, Zhejiang University, Hangzhou, Zhejiang 310058, China

ARTICLE INFO

Article history:
Received 27 September 2013
Received in revised form 2 December 2013
Accepted 2 December 2013
Available online 11 December 2013

Keywords:
Allosteric inhibitor
Binding free energy
Binding mechanism
Molecular dynamics simulation
Protein kinase B/PKB

ABSTRACT

Protein kinase B (PKB/Akt) is an attractive target for the treatment of tumor. Unlike PKB's ATP-competitive inhibitors, its allosteric inhibitors can maintain PKB's inactive state via its binding in a pocket between PH domain and kinase domain, which specifically inhibit PKB by preventing the phosphorylations of Thr308 and Ser473. In the present studies, MD simulations were performed on three allosteric inhibitors with different inhibitory potencies (IC_{50}) to investigate the interaction modes between the inhibitors and PKBα. MM/GB(PB)SA were further applied to calculate the binding free energies of these inhibitors binding to PKBα. The computed binding free energies were consistent with the ranking of their experimental bioactivities. The key residues of PKBα interacting with the allosteric inhibitor were further discussed by analyzing the different interaction modes of these three inhibitors binding to PKBα and by calculating binding free energy contributions of corresponding residues around the binding pocket. The structural requirements were then summarized for the allosteric inhibitor binding to PKBα. A possible structural mechanism of PKBα inhibition induced by the binding of allosteric inhibitor was formulated. The current studies indicate that there should be an optimum balance between the van der Waals and total electrostatic interactions for further designing of PKBα allosteric inhibitors.

1. Introduction

Protein kinase B (PKB, also known as Akt) is a key effector in the PI3K–Akt–mTOR pathway and plays a pivotal role in cell survival and proliferation [1,2]. As a member of AGC protein kinase superfamily, PKB shares 65% homology in the whole sequence and 80% residue identity in the ATP-binding pocket with protein kinase A (PKA). There are three subtypes of human PKBs, including PKBα/Akt-1, PKBβ/Akt-2, and PKBγ/Akt-3, which are encoded by different genes and share more than 80% sequence homology with each other [3,4]. PKB contains three domains, an N-terminal pleckstrin homology (PH) domain, a central catalytic domain, and a hydrophobic motif at the C-terminals. The PI3K–Akt–mTOR pathway starts from the phosphatidylinostiol-3-Kinase (PI3K) activation induced by G-protein coupled receptor or protein tyrosine kinase [5]. Activated PI3K catalyzes the phosphorylation of PtdIns(3,4)P2 (PIP2) to form PtdIns(3,4,5)P3 (PIP3) which can interact with the PH domain of PKB. PIP3-bound PKB is recruited to the plasma membrane for 3′-phosphoinositide-dependent kinase-1 (PDK1) catalyzed phosphorylation of Thr308 (in PKBα) located in the PKB activation loop. Then, mTORC2 promotes the phosphorylation of Ser473 located at the C-terminals next to the catalytic domain [4,6]. The phosphorylations at the residues of Thr and Ser of PKB are responsible for the full activation of PKB to regulate the survival, growth, proliferation, and metabolism of cell.

The aberrant activation of PKB has been widely implicated in many human cancers through several different mechanisms, including alterations of PI3K [7–11], alterations of the tumor suppressor phosphatase and tensin homolog (PTEN) [12–14], and alterations of PKB [10,15–19]. Therefore, it is expected that inhibition of PKB might prevent cellular growth and proliferation, and reverse the repression of apoptosis and resistance to cytotoxic agents in cancer cells [20]. Up to now, there are several kinds of compounds discovered to have good inhibitory activity to target PKBs. Some PKBα inhibitors have been in phase I or II clinical studies. According to the difference of their binding pockets in PKB, PKB's inhibitors can be classified into ATP-competitive inhibitor and allosteric inhibitor. The research group of Merck developed the allosteric inhibitors of PKBα and the corresponding inhibition model in 2005 [21]. Unlike ATP-competitive inhibitor docking to

Abbreviations: PKB/Akt, protein kinase B; MD, molecular dynamics; PI3K, phosphatidylinostiol-3-kinase; PDK1, 3′-phosphoinositide-dependent kinase-1; PTEN, phosphatase and tensin homolog; MM/PBSA, molecular mechanics/Poisson Boltzmann surface area; MM/GBSA, molecular mechanics/generalized Born surface area; PH, pleckstrin homology; RMSD, root-mean-square deviations; SMD, steered molecular dynamics.

* Corresponding author at: College of Pharmaceutical Sciences, Zijingang Campus, Zhejiang University, 866 Yuhangtang Road, Hangzhou, Zhejiang 310058, China. Tel.: +86 571 88208659.
E-mail address: chjz@zju.edu.cn (J.-Z. Chen).

1093-3263/$ – see front matter © 2013 Elsevier Inc. All rights reserved.
http://dx.doi.org/10.1016/j.jmgm.2013.12.002

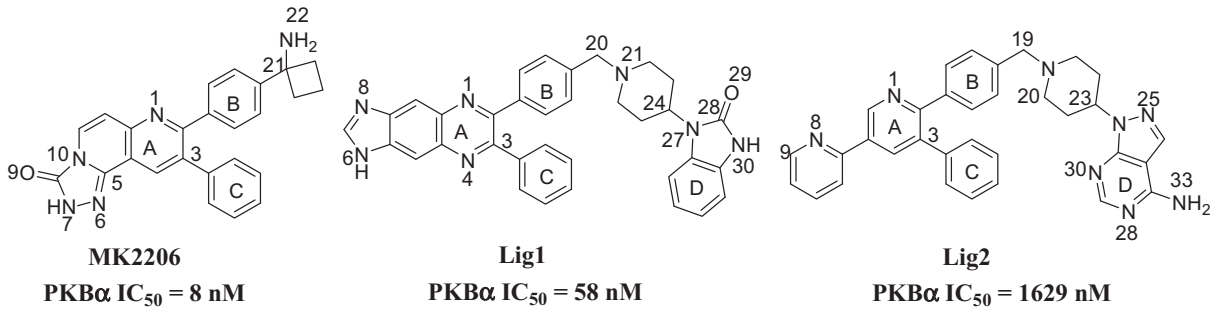

Fig. 1. The structures and IC_{50} values of PKBα's allosteric inhibitors MK2206 [22], Lig1 [23,24], and Lig2 [25].

the ATP-binding pocket of PKB, the allosteric inhibitor binds to a site that exists only in the presence of the PH domain for the stabilization of PKB in a "closed" conformation to prevent Thr308's phosphorylation promoted by PDK1 [1]. The allosteric inhibitor is selective against closely related kinases, like PKA or PKC, since it is non-competitive with respect to ATP and peptide substrate. Therefore, the PH domain-dependent allosteric inhibitor has gained great interest in the discovery and development of PKBα inhibitors in the past few years. Anticancer drug MK2206 [22] is an allosteric inhibitor currently studied in phase II trials for a combination treatment of metastatic solid tumors. As MK2206's analogs, inhibitors Lig1 (1-(1-(4-(7-phenyl-1H-imidazo[4,5-g]quinoxalin-6-yl)-benzyl)-piperidin-4-yl)-1H-benzo[*d*]-imidazol-2(3H-one) [23,24] and Lig2 (1-(1-(4-(5′-phenyl-2,3′-bi-pyridin-6′-yl)-benzyl)-piperidin-4-yl)-1H-pyrazolo[3,4-*d*]-pyrimidin-4-amine) [25] were also developed to be PKBα's allosteric inhibitors with modest and low bioactivity, respectively. The reported X-ray co-crystal structure [24] of PKBα with Lig1 showed the binding feature of Lig1 in the allosteric pocket of PKBα. Fig. 1 displays the chemical structures of these three inhibitors and their experimental bioactivities against PKBα.

The research group of Merck has successfully designed a series of allosteric inhibitors of PKBα [2,22,25–38]. Only one X-ray co-crystal structure [24] was reported for the allosteric inhibitor binding to PKBα. Calleja et al. elucidated the mechanism of PKBα allosteric inhibition through theoretical studies [39]. They used a multidisciplinary approach including molecular modeling and classical biochemical assays to depict the interactions of Lig1 with PKBα. It was found that Trp80 and Gln218 were important residues for maintaining the quaternary structure of PKBα in its inactive conformation. The PH domain induced cavity for the inhibitor's binding in PKBα was not formed in PKBγ. Gln218 was identified as an important residue for the stability of the Ser473 phosphorylation by molecular modeling and biochemical assays [24,39]. Due to the missing residues of Gly299–Thr312 in the activation loop of PKBα in its X-ray crystal structure, the Thr308 phosphorylation feature was analyzed and tested by biochemical assays to supply experimental data for the inhibitory effects of its allosteric inhibitors [39].

As reported, most allosteric PKBα inhibitors consist of an aromatic fused ring A, a six membered ring B, and a benzene ring C (Fig. 1). Recent studies [2,22,25–38] have shown that the biological activities vary with the substitution positions of ring and nitrogen atom on the aromatic fused ring A and the primary amino group of MK2206, indicating that the structural difference of inhibitors affects significantly their binding processes to PKBα. This may be caused by a specific conformation in the kinase domain which is induced by the inhibitor's binding to a pocket near PH domain of PKB. Therefore, the allosteric inhibitor has an absolutely pharmacophoric requirement for its binding to PKBα. It needs a detailed perspective into the interactions happened between PKBα and allosteric inhibitors. It would be significant to understand the influence of a specific conformation of PKB's allosteric inhibitor on the dynamic characteristics of its bound state.

As an important technology and tool to study interaction mechanism of ligand-receptor complex, molecular dynamics (MD) simulations and free energy calculation studies on the binding mechanism of different kinase inhibitors have received much attention in recent years [40,41]. By integrating molecular mechanics energy and continuum solvation models, molecular mechanics/Poisson Boltzmann surface area (MM/PBSA) [42] and molecular mechanics/generalized Born surface area (MM/GBSA) [43] were developed for the free-energy calculations and molecular docking studies of ligand binding to its target protein. MM/PBSA and MM/GBSA are indeed more specific than most empirical or knowledge-based scoring functions. In the current study, MD simulations and MM/PB(GB)SA free energy calculations were performed to three allosteric inhibitors MK2206, Lig1, and Lig2, respectively, binding to PKBα. We investigated the interaction features between PKBα and these inhibitors to understand the specificity of the allosteric inhibitor binding to PKBα. The key residues interacting with the allosteric inhibitor were discussed by analyzing the different interaction modes of these three inhibitors, with different inhibitory potencies, binding to PKBα and by comparing the different binding free energy contributions of corresponding residues around the binding pocket. The pharmacophoric requirements were then summarized for the allosteric inhibitor binding to PKBα. It is expected that this work will provide helpful information for the design of novel and potent allosteric inhibitors of PKBα.

2. Methods and computational details

2.1. System preparation

The X-ray co-crystal structure of PKBα-Lig1 (PDB entry: 3O96 [24]), downloaded from the RCSB Protein Data Bank (PDB), was applied to be the initial structure for the current molecular dynamic simulations. The missing residues (Asp46–Arg48, His89–Glu91, Glu114–Arg144, Lys189–Glu198, Gly299–Thr312) of PKBα in the crystal structure were inserted by using the loop search algorithm in BIOPOLYMER module of SYBYL x1.3 [46]. The structure was then finalized by adding hydrogen atoms, assigning partial charges and protonation states using the BIOPOLYMER module of SYBYL x1.3 [46] and the energy minimization was performed on the generated structure with 1000 steps of steepest descent to relax amino residue side chains. The obtained structure was regarded as the starting point for the following calculations. The initial structural models of complexes PKBα-MK2206 and PKBα-Lig2 were derived from the above treated structure of PKBα-Lig1. Either MK2206 or Lig2 was respectively prepared by modifying the structure of Lig1 extracted from above PDB file using the Sketch module of SYBYL x1.3 [46]. The in silico generated conformation of Lig2 or MK2206 was then merged into the binding pocket of the complex PKBα-Lig1

to replace Lig1 for the generation of preliminary structural models of the complexes PKBα-MK2206 and PKBα-Lig2, respectively.

2.2. Molecular dynamics simulations

Molecular dynamics simulations were performed on the above three complexes, respectively, using AMBER11 software package [47]. The generated structural model of each complex was first immersed in a 9.0 Å truncated octahedron periodic water box to get corresponding solvation model. LEaP protocol [48] was applied to add Na^+ counterions for the neutralization of the system. The AMBER03 force field [49] was applied for the potentials of the proteins, while the general AMBER force field (GAFF) [50] was used to establish the potentials of the inhibitors. The atom types and atomic charges were reassigned by the Antechamber tool in the Amber software package [47].

Prior to MD simulations, structural optimizations were first performed on each system for the relaxation of any steric conflicts produced during system setup. Energy minimizations were carried out for three steps. At first two steps, all of waters and counterions were relaxed, while all heavy atoms of both PKB and inhibitor were restrained with a harmonic constraint potential of 500 kcal/mol Å^2 and then with a reduced harmonic constraint potential of 10.0 kcal/mol Å^2, respectively. Finally, the whole system was relaxed without any restraint. The three steps above all feature 2500 cycles of steepest descent followed by 5000 cycles of conjugate gradient minimization.

After minimization, MD simulations were performed on each system. During MD calculations, Particle Mesh Ewald (PME) [51] was employed to deal with the long-range electrostatic interactions. A cutoff distance of 10.0 Å was applied for the calculation of the long-range van der Waals (vdW) energy term. The SHAKE procedure was applied and the time step was set to 2 fs [52]. At first, each system was gradually heated from 0 to 300 K in 100 ps in an NVT ensemble. The coupling coefficient was set as 1.0 ps^{-1} [53]. During the heating process, the systems were restrained with a force constant of 10 kcal/mol Å^2. Additional 400 ps MD equilibrations were performed with decreasing restraint weights of 5 kcal/mol Å^2, 1 kcal/mol Å^2, 0.5 kcal/mol Å^2, and 0.1 kcal/mol Å^2, respectively, in each time period of 100 ps at 300 K. At last, 20 ns MD productions were performed for each system at 300 K. Coordinate trajectories were saved every 1 ps throughout the equilibration runs and every 2 ps throughout the production runs. For each system, 1000 conformations from the last 2 ns MD trajectory were extracted for further binding free energy calculations and decomposition analyses.

2.3. Calculation of binding free energy of inhibitor binding to PKBα

The binding free energies (ΔG_{bind}) of the inhibitors with PKBα were calculated by MM/PB(GB)SA method using Amber11 [47]. It can be calculated using the following equation:

$$\Delta G_{bind} = G_{complex} - (G_{protein} + G_{ligand}) = \Delta H - T\Delta S \quad (1)$$

$$\Delta G_{bind} = \Delta E_{MM} - T\Delta S + \Delta G_{sol} \quad (2)$$

$$\Delta G_{bind} = \Delta E_{noncovlent} + \Delta E_{covlent} - T\Delta S + \Delta G_{sol} \quad (3)$$

$$\Delta G_{bind} = \Delta E_{ele} + \Delta E_{vdW} - T\Delta S + \Delta G_{ele,\ sol\ PB(GB)} + \Delta G_{nonpol,\ sol} \quad (4)$$

As indicated in Eq. (1), the binding free energy can be calculated as the *D*-value of the free energies of PKBα-inhibitor complex ($G_{complex}$) and PKBα ($G_{protein}$) and inhibitor (G_{ligand}). According to molecular mechanic theory, the force field (ΔE_{MM} in Eq. (2)) to calculate the interaction energy of inhibitor binding to PKBα can represent the enthalpic component of free energy. As a reversible inhibitor binding to PKBα, the allosteric inhibitor would only have non-covalent interaction ($\Delta E_{noncovlent}$ in Eq. (3)), which is composed of electronic item (ΔE_{ele} in Eq. (4)) and van der waals energy (ΔE_{vdW} in Eq. (4)), but no covalent one ($\Delta E_{covlent} = 0$) with its target protein PKBα.

The solvation free energy ΔG_{sol}, included in Eq. (3), was calculated by MM/PB(GB)SA method integrating the molecular mechanical energies with the continuum solvent approaches. As illustrated in Eq. (4), ΔG_{sol} is composed of an electrostatic contribution ($\Delta G_{ele,\ sol\ PB(GB)}$) and a nonpolar contribution ($\Delta G_{nonpol,\ sol}$). $\Delta G_{ele,\ sol\ PB(GB)}$ was estimated with 1000 representative snapshots extracted from the last 2 ns MD trajectory using a Poisson Boltzmann (PB) model [54] or a generalized Born (GB) model [55]. $\Delta G_{nonpol,\ sol}$ accounts for the solvation effects and can be calculated by relating it to the solvent accessible surface area (SASA) [56]. The SASA (Å^2) was calculated with a probe radius of 1.4 Å for both PB and GB methods, which gets the solvent excluded surface. The molsurf program [57] and the LCPO (linear combination of pairwise overlaps) method [56] were applied to calculate the SASA in the PBSA and GBSA methods, respectively. $\Delta G_{nonpol,\ sol}$ was calculated as Eq. (5) with a surface tension parameter γ constant of 0.0378 kcal/mol Å^2 and a parameterized *b* value of −0.5692 kcal/mol for PB computation [58] and corresponding γ constant of 0.0072 kcal/mol Å^2 and b value of 0 kcal/mol for GB calculations [59].

$$\Delta G_{nonpol,sol} = \gamma SASA + b \quad (5)$$

Finally, entropy contributions $T\Delta S$ to the total free energy may be added as a further refinement. The entropy contributions (translation, rotation, and vibration) were obtained by using the Nmode protocol [60]. It can be determined from the following equation:

$$T\Delta S = T(\Delta S_{trans} + \Delta S_{rot} + \Delta S_{vib}) \quad (6)$$

We applied 40 snapshots, which were used for previous computation of the solvation free energies, extracted from the last 2 ns MD trajectory to calculate the entropic contributions. The minimization for each snapshot was carried out using the conjugated gradient method with a distance-dependent dielectric of $4r_{ij}$ (r_{ij} is the distance between two atoms) until the root-mean-square of the elements of the gradient vector was lower than 1.0×10^{-4} kcal/mol Å.

The experimental binding free energy was calculated on the basis of the inhibitory activity of IC_{50} using the following equation [61]:

$$\Delta G_{exp} \approx -RT \cdot \ln\ IC_{50} \quad (7)$$

where $R = 1.986 \times 10^{-3}$ kcal/K mol, $T = 300$ K, and IC_{50} is in a molar unit.

2.4. Calculation of the inhibitor–residue interaction

To obtain more information about the energetic profile of the interaction during the MD trajectory, per-residue binding free-energy decomposition was performed using the MM/GBSA program in Amber11 [47]. The binding interaction of each inhibitor–residue pair includes three energy terms: van der Waals contribution (ΔG_{vdW}), electrostatic contribution (ΔG_{ele}) and solvation contribution (ΔG_{sol}). The solvation free energy ΔG_{sol} was computed as the sum of the polar ($\Delta G_{ele,\ sol}$) and the non-polar ($\Delta G_{nonpol,\ sol}$) parts.

$$\Delta G_{inhibior\text{-}residue} = \Delta G_{MM} + \Delta G_{sol} = \Delta E_{vdW} + \Delta E_{ele} + \Delta G_{ele,\ sol} + \Delta G_{nonpol,\ sol} \quad (8)$$

Table 1
Hydrogen bonds analysis from MD simulations.[a]

System	Donor	Acceptor	Occupancy (%)[b]	Distance (Å)[c]
PKBα-MK2206	ligand N7-H	Ser205 O	99.09	2.93 (0.16)
	ligand N22-H	Gln79 O	86.34	2.76 (0.15)
	ligand N22-H	Thr82 O	20.37	4.82 (0.13)
	ligand N7-H	Tyr263 O	16.47	3.47 (0.50)
PKBα-Lig1	ligand N6-H	Ser205 O	98.76	3.03 (0.24)
PKBα-Lig2	ligand N33-H	Glu85 O	46.33	2.86 (0.23)
	ligand N33-H	Glu17 OE1	20.67	2.85 (0.32)
	ligand N33-H	Glu17 OE2	19.57	3.30 (0.35)

[a] The listed donor and acceptor pairs satisfy the criteria (H-bond length less than 5 Å and H-bond angle in the range of 120–180°) for the hydrogen bond over 10.0% of the time during the 20 ns of simulation.
[b] Occupancy is the percentage of H-bond formed during the investigated time period.
[c] The average distance with standard error (SE = standard deviation/$N^{1/2}$) in parentheses between H-bond acceptor atom and H-bond donor atom in the investigated time period.

Like Eq. (1), ΔE_{vdW} and ΔE_{ele} could be calculated with the sander program in Amber11 [47]. $\Delta G_{ele,\,sol}$ was calculated by the generalized Born (GB) model with the parameters developed by Aguilar et al. [62]. $\Delta G_{nonpol,\,sol}$ was computed on the basis of SASA which was determined with the ICOSA method [63]. The same snapshots were used for per-residue free energy decomposition analysis.

3. Results and discussion

3.1. Equilibrium of the MD simulations

Twenty nanosecond MD simulations have been successfully performed on each of three complexes, including PKBα-MK2206, PKBα-Lig1, and PKBα-Lig2, in solvation environment. In order to ensure the rationality of the MD simulated results, we first compared the representative snapshots of each system taken from last 2 ns MD trajectory with the X-ray co-crystal structure of PKBα-Lig1. As illustrated in Fig. 2, the binding mode of Lig1 from MD simulated result is nearly the same as that of Lig1 extracted from the X-ray co-crystal structure. Both Lig2 and MK2206 share a similar binding mode with Lig1 in PKBα. These three ligands are all stabilized in the PH domain-dependent allosteric pocket, which is formed by the residues of Glu17, Gln79, Trp80, Thr82, Glu85, Ser205, Tyr263, Tyr326, and Tyr272. Those main amino acid residues which can form hydrogen bonds with the inhibitor are supported by the results from H-bond analyses (Table 1).

It can reflect the dynamic stabilities of the three complexes using the values of root-mean-square deviations (RMSD) for all Cα atoms of protein, backbone atoms of residues in the binding pocket within 6.5 Å around each inhibitor, and all heavy atoms of each inhibitor. The RMSDs of each of three systems relative to their initial minimized structures were calculated and plotted in Fig. 3a and c during the whole period of MD simulation. As displayed in Fig. 3a–c, the RMSDs of each system tend to stabilize after 5 ns of the simulation phase, indicating the systems reached the equilibrium. Therefore, it is reasonable to do the binding free energy calculation and free energy decomposition based on the conformations extracted from 18 to 20 ns. In the meantime, Fig. 3 also indicates that the fluctuations of the three systems are very similar during MD simulation. The RMSDs of the complexes fluctuate around ~3.5 Å, ~2.0 Å and ~1.0 Å for protein, binding pocket and ligand, respectively. The result indicates that the three complexes have stable protein structures, same binding pockets, and similar binding modes. Although the RMSD fluctuations of MK2206 are different from those of Lig1 and Lig2 after 5 ns, the binding conformation of MK2206 is stable. As illustrated in Fig. 4, the cyclobutylamine group linked on the C21 atom of MK2206 rotates about 90° away from the original position from 5 ns to 15 ns to induce NH_2 group forming H-bond interactions with the backbone chain carbonyl groups of both Gln79 and Thr82. After 15 ns MD simulations, 1-cyclobutylamine group of MK2206 rotates back about 45° toward the original position making its NH_2 have H-bond interactions with the side chain carbonyl group of Gln79 and the backbone chain carbonyl group of Thr82, which is similar to the initial structure.

The value of root-mean-square fluctuation (RMSF) is another tool to monitor the dynamic stability of the three systems. RMSF can reflect the mobility of the residue around its mean position. Fig. 3d illustrates the RMSF values versus the residue number for complexes. The RMSF values of the X-ray co-crystal structure of PKBα-Lig1 were also obtained by the transformation of the experimental B-factors in the crystal structure. As described in the *Method* section, we supplied the structural model of PKBα's missing residues (Asp46–Arg48, His89–Glu91, Glu114–Arg144, Lys189–Glu198, Gly299–Thr312) in PDB entry 3O96 on the basis of its crystal structure. The structure of PKBα-Lig1 from MD simulations shares similar RMSF distributions to the X-ray co-crystal structure of PKBα-Lig1. It could be hypothesized that the residues missed in the crystal structure of PKB would not influence the allosteric inhibitor binding to the active pocket of PKB during MD simulation. RMSFs of the residues near the missing loops also show similar trend between MD values and experimental data. Accordingly, the structures of the three systems from MD results share similar RMSF distributions and similar trends of dynamic features, including the residues in the flexible loops with higher fluctuation values (Fig. 3d). This result shows that the MD simulation trajectories of the three complexes would be reliable for the post analyses.

3.2. Comparison of binding free energies

After 20 ns MD simulations, a total of 1000 snapshots were taken at an interval of 2 ps from the last 2 ns MD trajectory for further binding free energy calculations and decomposition analyses. First, the MM/PB(GB)SA methods in AMBER 11 [47] were used to calculate the binding free energies of the three systems. Table 2 summarizes the binding free energy and its contributed components computed by MM/PB(GB)SA, and the entropy contributions obtained by using the Nmode protocol [60], for each system. As listed in Table 2, the MM/PBSA calculated binding free energies ($\Delta G_{pred\,(PB)}$) are −64.73, −46.40, and −37.53 kcal/mol for MK2206, Lig1, and Lig2, respectively, binding to PKBα, while the MM/GBSA computed binding free energies ($\Delta G_{pred\,(GB)}$) are −32.70, −29.91, and −26.48 kcal/mol for MK2206, Lig1, and Lig2, respectively, binding to PKBα. Comparing to the experimental binding free energies (ΔG_{exp}: MK2206, −11.11 kcal/mol; Lig1, −9.93 kcal/mol; and Lig2, −7.94 kcal/mol) determined based on their IC_{50} values (PKBα inhibitory potency: MK2206, IC_{50} = 8 nM [22]; Lig1, IC_{50} = 58 nM [23,24]; and Lig2, IC_{50} = 1629 nM [25]), the ranking of simulated binding free energies is consistent with their experimental data, although the MM/PB(GB)SA calculated binding free energies do not

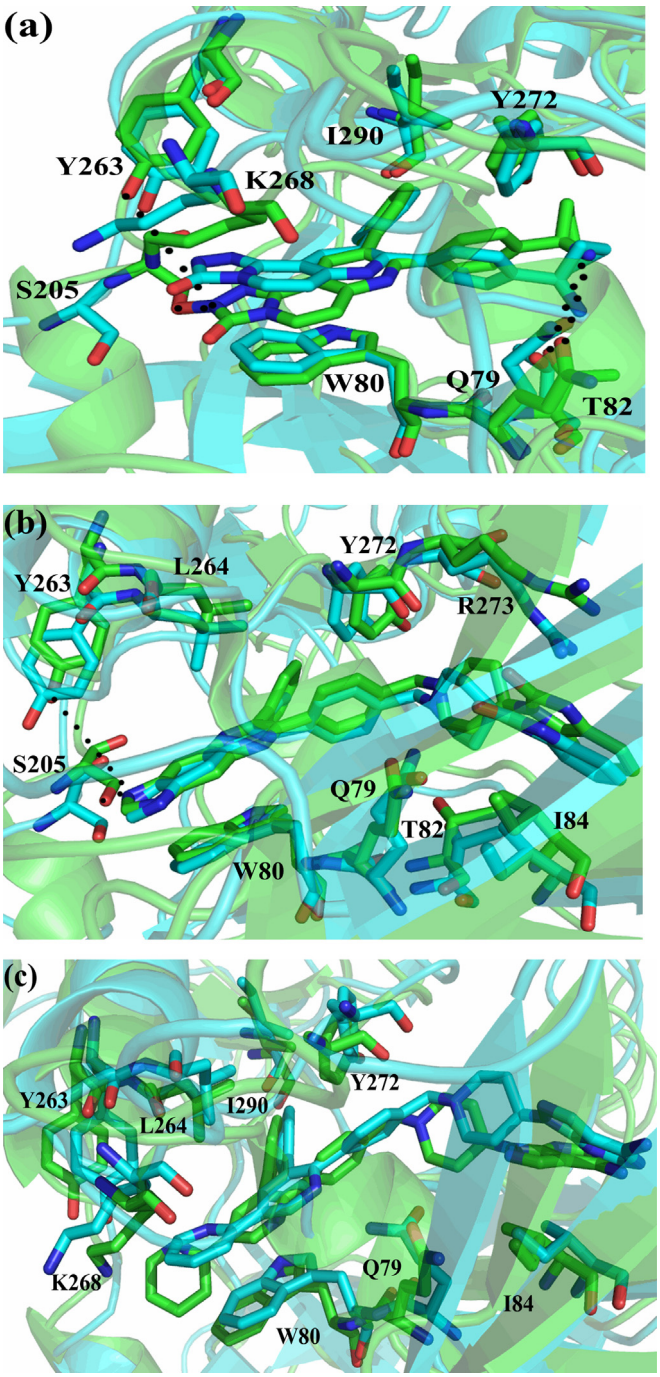

Fig. 2. Structural comparison between initial (green) and MD simulated representative snapshots (cyan) of (a) MK2206, (b) Lig1, (c) Lig2 at the active site of PKBα. Black dots represent hydrogen bonds.

match the absolutely experimental values accurately. According to the calculated $\Delta G_{\text{pred(PB/GB)}}$ values, the most potent inhibitor MK2206 has the lowest binding free energies among the three inhibitors, which means that MK2206 binds more tightly to PKBα than both Lig1 and Lig2. This is in accord with the fact that MK2206 has the best bioactivity among the three inhibitors. Therefore, MM/PB(GB)SA calculated results would be reliable for the analyses of the interaction mode and the structural mechanism of allosteric inhibitor binding to PKBα.

In order to understand the structural mechanism of the inhibitors in detail, the binding free energies of each system were further decomposed into individual components by either

Table 2
Binding free energies and its components for the studied inhibitors with proteins.[a]

Protein-inhibitor	PKBα-MK2206	PKBα-Lig1	PKBα-Lig2
$\Delta G_{\text{pred (PB)}}$	−64.73	−46.40	−37.53
$\Delta H_{\text{(PB)}}$	−80.17	−70.19	−62.40
$\Delta E_{\text{vdW}} + \Delta G_{\text{nonpol, sol (PB)}}$	−90.40	−126.42	−116.37
$\Delta G_{\text{nonpol, sol (PB)}}$	−38.01	−49.06	−47.02
$\Delta E_{\text{ele}} + \Delta G_{\text{ele, sol (PB)}}$	10.25	56.24	53.97
$\Delta G_{\text{ele, sol (PB)}}$	183.70	64.81	159.42
$\Delta G_{\text{pred (GB)}}$	−32.70	−29.91	−26.48
$\Delta H_{\text{(GB)}}$	−48.14	−53.70	−51.35
$\Delta E_{\text{vdW}} + \Delta G_{\text{nonpol, sol (GB)}}$	−58.74	−85.54	−77.67
$\Delta G_{\text{nonpol, sol (GB)}}$	−6.35	−8.18	−8.32
$\Delta E_{\text{ele}} + \Delta G_{\text{ele, sol (GB)}}$	10.61	31.84	26.33
$\Delta G_{\text{ele, sol (GB)}}$	184.06	40.41	131.78
ΔE_{vdW}	−52.39	−77.36	−69.35
ΔE_{ele}	−173.45	−8.57	−105.45
$T\Delta S$	−15.44	−23.79	−24.87
ΔG_{exp}	−11.11	−9.93	−7.94
IC_{50} (nM)	8.00	58.00	1629.00

[a] All energies are in kcal/mol. ΔH: the enthalpy changes, $\Delta H = \Delta E_{\text{ele}} + \Delta E_{\text{vdW}} + \Delta G_{\text{nonpol, sol}} + \Delta G_{\text{ele, sol}}$. $T\Delta S$: the entropy changes. ΔG_{pred}: the calculated binding free energy by MM-PB(GB)SA method. ΔG_{exp}: the experimental binding free energy calculated according to the IC_{50} by $\Delta G \approx -RT \cdot \ln IC_{50}$. The IC_{50} values of MK2206, Lig1, and Lig2 were taken from references [22–25].

MM/PBSA or MM/GBSA methods in AMBER 11 [47]. As indicated in Table 2, the components ΔE_{vdW}, ΔE_{ele}, and $\Delta G_{\text{nonpol, sol}}$ drive the favorable interactions between PKBα and each of three ligands. Both MM/PBSA and MM/GBSA calculations indicate that solvation electrostatic interaction contributions ($\Delta G_{\text{ele, sol (PB)}}$ or $\Delta G_{\text{ele, sol (GB)}}$) are unfavorable within the three systems. The contributions of entropy changes ($-T\Delta S$) to the free energies impair the binding of each inhibitor to PKBα. By analyzing the free energy components of either highly potent MK2206 or lowly active Lig2 binding to PKBα, it is revealed that both ΔE_{vdW} and $\Delta G_{\text{nonpol, sol}}$ drive the favorable interactions for both MK2206 and Lig2 binding to PKBα. There are two typically hydrophobic interactions formed between the aromatic ring A and the indole ring of Trp80 and between the phenyl ring B and the phenyl ring of Tyr272 for both MK2206 (Fig. 2a) and Lig2 (Fig. 2c). By comparison with the short cyclobutyl group of MK2206, the extended 1*H*-pyrazolo-[3,4-*d*]-pyrimidine group of Lig2 can form another hydrophobic interaction with the phenyl ring of residue Tyr326 (Fig. 2b). Obviously, ΔE_{vdW} and $\Delta G_{\text{nonpol, sol}}$ of PKBα-Lig2 contribute more to the ligand's binding than those of PKBα-MK2206. On the other hand, electrostatic interaction (ΔE_{ele}) contributes more to either MK2206 or Lig2 binding to PKBα than ΔE_{vdW} and $\Delta G_{\text{nonpol, sol}}$. The most noticeable differences between MK2206 and Lig2 also lie in electrostatic interactions. As listed in Table 1, MK2206 can make very strong hydrogen bond interactions with the residues Gln79, Thr82, Ser205, and Tyr263 of PKBα, while Lig2 can only form H-bonds with another two charged residues Glu17 and Glu85 which are nearly located at the surface of PKBα (Fig. 2c). The resulting electrostatic interaction contributions in vacuum and solvent ($\Delta E_{\text{ele}} + \Delta G_{\text{ele, sol}}$) for MK2206 are also more favorable than those for Lig2. As to Lig1, there is a hydrogen bond interaction between Lig1 and residue Ser205. The contributions of van der Waals and nonpolar solvation energies are mainly responsible for Lig1 to bind to PKBα. The contributions of van der Waals and nonpolar solvation energies for Lig1 are more than those for either MK2206 or Lig2. The more contributions of ΔE_{vdW} and $\Delta G_{\text{nonpol, sol}}$ may lead to the better bioactivity of Lig1 than that of Lig2. However, the predicted electrostatic interaction contributions in vacuum and solvent ($\Delta E_{\text{ele}} + \Delta G_{\text{ele, sol}}$) of PKBα-Lig1 are more unfavorable than those of PKBα-MK2206. This probably leads to the higher bioactivity of MK2206 than Lig1. The results of free-energy decomposition

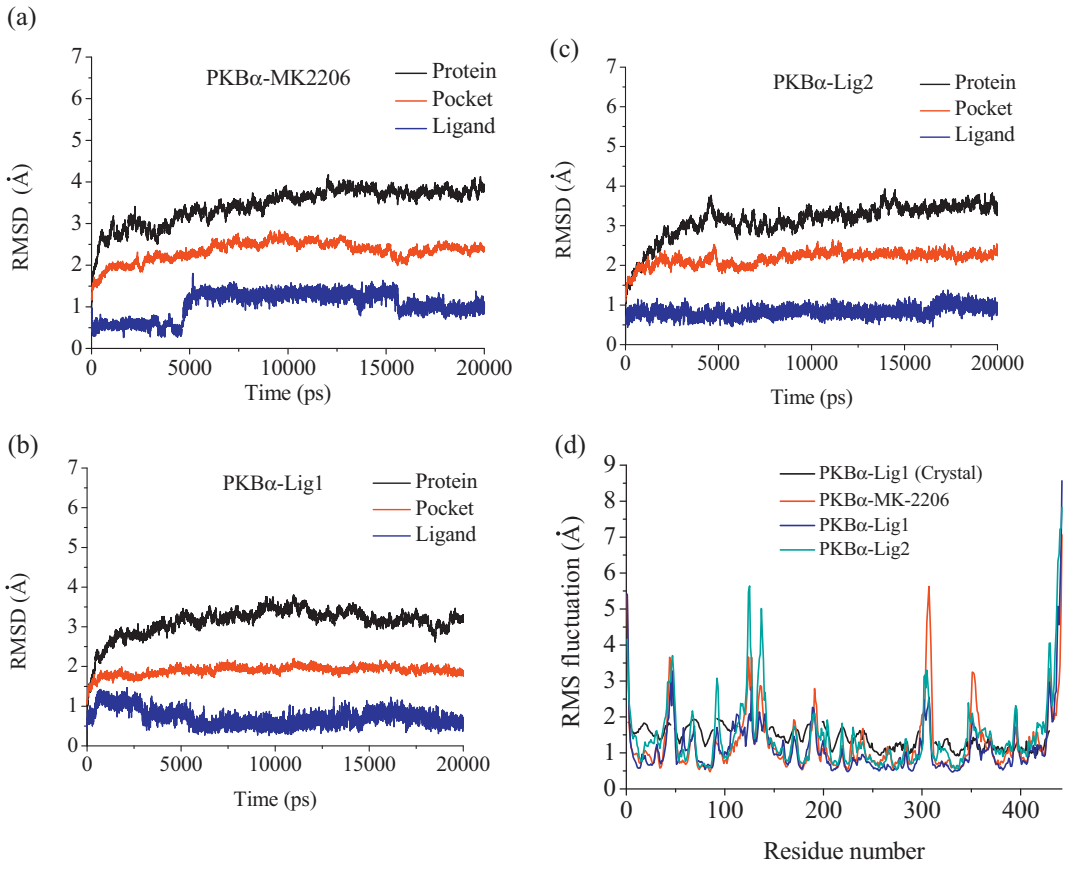

Fig. 3. RMSDs of Cα atoms of the protein, backbone atoms of binding pocket (within 6.5 Å), and the heavy atoms in the ligand for (a) PKBα-MK2206, (b) PKBα-Lig1, (c) PKBα-Lig2, (d) RMSF of each residue of the protein for the complex obtained from the crystal structure and all three PKBα complexes obtained from 20 ns MD simulation.

calculations agree well with the experimental values, suggesting that there should be an optimum balance between total electrostatic and hydrophobic interactions for the designing of PKBα allosteric inhibitors.

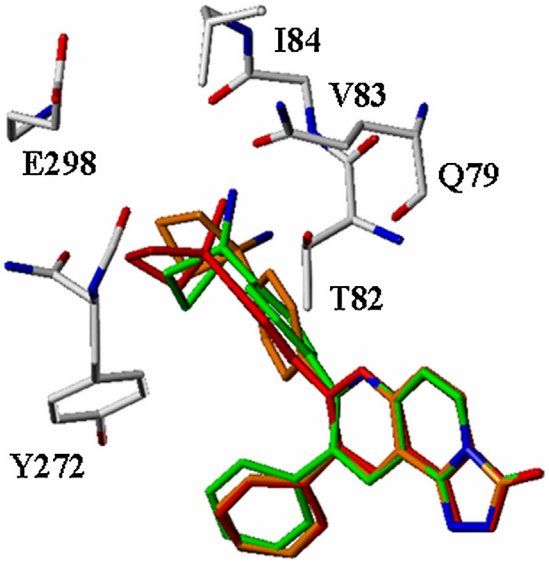

Fig. 4. Structure comparison between representative snapshots of MK2206 from MD results of 2 ns (green), 12 ns (orange) and 20 ns (red). (For interpretation of the references to color in this figure legend, the reader is referred to the web version of the article.)

3.3. Analyses of interaction modes of allosteric inhibitors binding to PKBα

Pharmacophoric features are necessary structural pieces of a ligand to ensure the optimally steric and electronic interactions with a specific biological target and to trigger (or block) its biological response. The co-crystal structure of a ligand binding to its receptor protein illustrates their directly interactional mode. Therefore, the co-crystal structure of PKBα with its allosteric inhibitor Lig1 was applied as a starting point to do MD simulations of the interaction modes between PKBα and the three allosteric inhibitors with different bioactivities and the corresponding binding free energy calculations and the inhibitor–residue interaction computations. The important pharmacomphoric features embedded in currently studied allosteric inhibitors would be figured out by analyzing the interaction modes between each inhibitor and PKBα in our MD-simulated structural models of complexes of three PKBα's allosteric inhibitors, with different inhibitory activities, binding to PKBα. Such analyses would also help to propose the essential structure requirements, which are critical for improving the binding affinity with PKBα and the future design of potent and selective allosteric inhibitors.

By comparing the MD simulated interaction modes of highly potent inhibitor MK2206 and moderately active inhibitor Lig1, respectively, binding to PKBα, it can be seen that their structural difference do not induce largely variant interaction modes of these two inhibitors with PKBα. As listed in Table 1 for the H-bond analyses, the C-21 linked primary amino group of MK2206 can form hydrogen bond interactions with the side chain carbonyl group of Gln79 and the O atom of the hydroxyl group of Thr82. The N7-H group in [1,2,4]triazolo-[3,4-*f*]-[1,6]naphthyridin-3(2*H*)-one ring

of MK2206 also has hydrogen bond interactions with the O atoms of both the hydroxyl group of Tyr263 and the backbone carbonyl group of Ser205 with occupancies more than 10%. As shown in Fig. 2b, the N6-H group of Lig1 only forms one strong hydrogen bond interaction with the backbone carbonyl group of Ser205. Either inhibitor MK2206 or Lig1 has an H-bond interaction with the backbone carbonyl group but not side chain hydroxyl group of Ser205, which could explain why the experimental mutation S205A, carried out by Calleja et al. [64], did not affect the sensitivity of PKBα for the allosteric inhibitor. Another two H-bonds are formed between the O29 atom of Lig1 and the NH_2 group in the side chain amide group of Gln79, between the N21 atom of Lig1 and the hydroxyl group of Thr82 with occupancies less than 10% (not listed in Table 1). Therefore, Lig1 has obviously weaker hydrophilic interaction with PKBα than MK2206. These results indicate that the residues Gln79, Thr82, and Tyr263 of PKBα could play critical roles to have electrostatic interaction with its allosteric inhibitor.

In addition, hydrophobic interactions are also presented between PKBα and its inhibitors. It can be seen that the [1,2,4]triazolo[3,4-*f*][1,6]naphthyridin-3(2*H*)-one ring of MK2206 can form a stable π–π interaction with the indole ring of Trp80 since these two aromatic rings are almost parallel. Trp80 has been confirmed to be an important residue for allosteric inhibitor's locking PKB in its PH-in conformer by experimental mutation W80A performed by Calleja et al. [39,65]. There is also a hydrophobic interaction formed between the cyclobutyl group linked on the C21 atom of MK2206 and the methyl group in the side chain of Thr82. The phenyl ring C of MK2206 forms a hydrophobic interaction with the side chain of Ile290. In the meantime, the [1,2,4]triazolo[3,4-*f*][1,6]-naphthyridin-3(2*H*)-one ring and the phenyl group B of MK2206 can form hydrophobic but not stacking interactions with the phenyl groups of residues Tyr272 and Tyr263, respectively, since the corresponding aromatic rings are not parallel. Comparing to MK2206, Lig1 has similar hydrophobic interactions with PKBα. As illustrated in Fig. 2b, the 1*H*-imidazo[4,5-*g*]-quinoxaline ring of Lig1 can also have a parallel π–π interaction with the indole ring of Trp80. The 1*H*-imidazo[4,5-*g*]-quinoxaline ring A and phenyl group C of Lig1 form hydrophobic interactions with the phenyl groups of Tyr272 and Tyr263, respectively. Therefore, there are similar hydrophobic interaction patents presented in both MK2206 and Lig1 binding to PKBα.

However, the per-residue energy decomposition calculations indicate that above residues have different free energy contributions to inhibitors MK2206 and Lig1, respectively, binding to PKBα. As shown in Fig. 5a and b, although Ser205 has a little more energy contribution to Lig1 (−3.29 ± 0.02 kcal/mol) than MK2206 (−1.45 ± 0.02 kcal/mol), another three hydrophilic residues Gln79, Thr82, and Tyr263, which have H-bond interactions with MK2206 but not Lig1 as discussed above, have more energy contributions to MK2206 (Gln79: −4.26 ± 0.02 kcal/mol, Thr82: −5.43 ± 0.02 kcal/mol, and Tyr263: −1.84 ± 0.02 kcal/mol) than Lig1 (Gln79: −1.61 ± 0.02 kcal/mol, Thr82: −0.83 ± 0.02 kcal/mol, and Tyr263: −0.52 ± 0.02 kcal/mol). Among the hydrophobic residues in the binding pocket of PKBα, the residue Trp80 has the biggest energy contribution to either MK2206 (−5.21 ± 0.02 kcal/mol) or Lig1 (−5.07 ± 0.02 kcal/mol) binding to PKB, since it can have strong aromatic stacking interactions with aromatic fused ring As of these two inhibitors, respectively, as discussed above. Another two residues, Tyr272 and Tyr263, provide more favorable hydrophobic interactions to MK2206 than Lig1. The per-residue energy decomposition indicate that their energy contributions are −2.54 ± 0.02 kcal/mol (Tyr272) and −1.84 ± 0.02 kcal/mol (Tyr263) to MK2206 but only −0.45 ± 0.01 kcal/mol (Tyr272) and −0.52 ± 0.01 kcal/mol (Tyr263) to Lig1. Other hydrophobic residues, like Leu210 (MK2206: −1.83 ± 0.02 kcal/mol, Lig1: −1.83 ± 0.02 kcal/mol), and Ile290

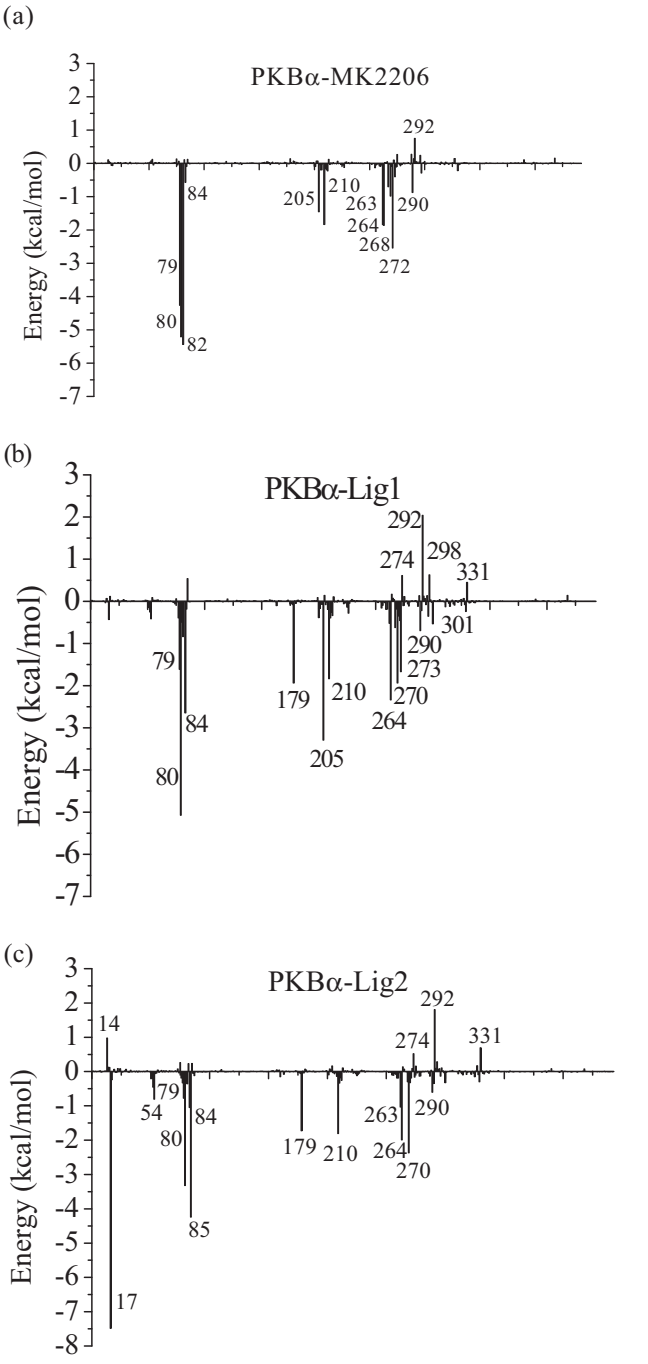

Fig. 5. Inhibitor–residue interaction spectra (a) PKBα-MK2206, (b) PKBα-Lig1, (c) PKBα-Lig2.

(MK2206: −0.87 ± 0.02 kcal/mol, Lig1: −0.69 ± 0.02 kcal/mol), provide similarly favorable hydrophobic interactions to both MK2206 and Lig1. As shown in Fig. 6a, the residues Trp80, Leu210, Tyr263, Tyr272, and Ile290 of PKBα make more contributions of van der Waals and nonpolar solvation energies to MK2206 than Lig1. The total electrostatic energies of Gln79, Thr82, and Tyr263 yield the energetic differences between MK2206 and Lig1 (Fig. 6b).

By comparing to MK2206 and Lig1, lowly bioactive inhibitor Lig2 has different interaction patent with PKBα since it has a quite different molecular structure. As illustrated in Fig. 5c and Table 1, the primary amino group of Lig2 can form two hydrogen bond interactions with the carboxyl groups in the side chains of Glu17 (−7.48 ± 0.02 kcal/mol) and Glu85 (−4.24 ± 0.02 kcal/mol),

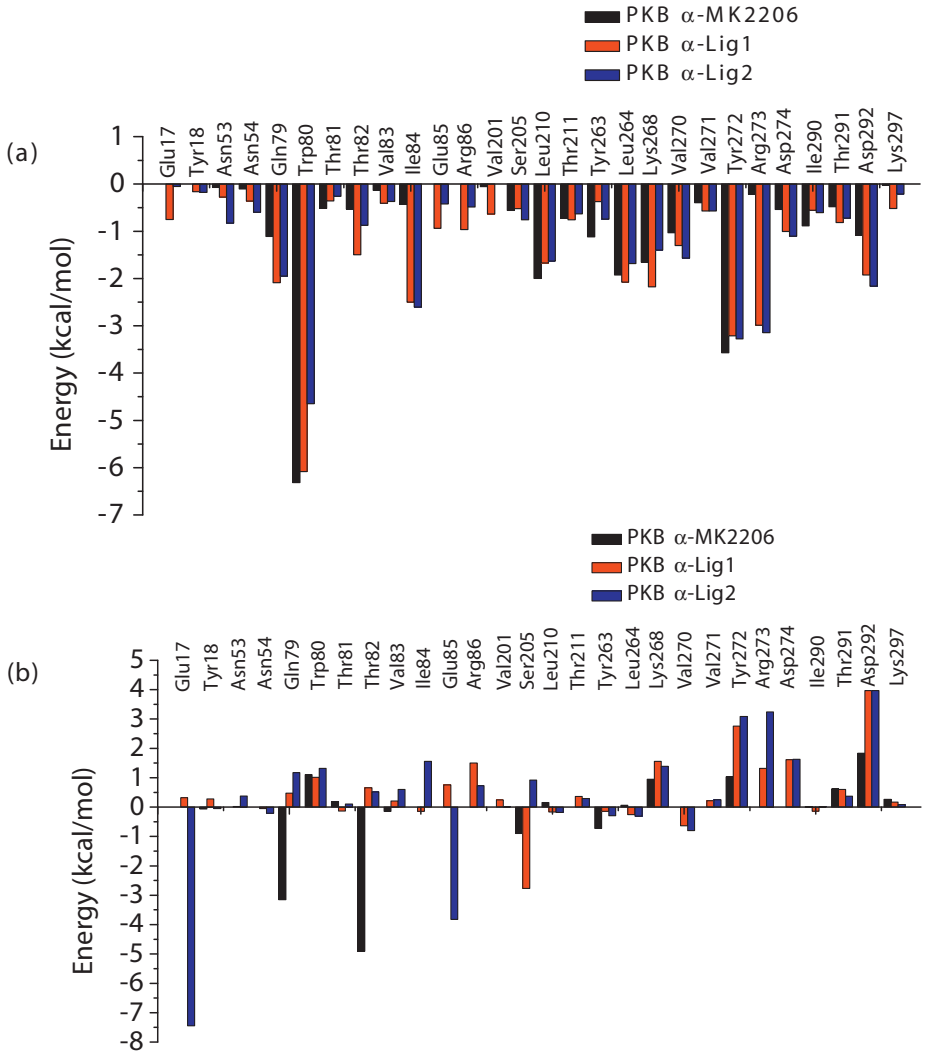

Fig. 6. Comparison of per-residue energy decomposition for key residues for the three systems, (PKBα-MK2206: black, PKBα-Lig1: red, PKBα-Lig2: blue): (a) the sum of vdW and nonpolar solvation energy, $\Delta G_{vdW} + \Delta G_{nonpol,\,sol}$, and (b) the sum of electrostatic and polar solvation energy, $\Delta G_{ele} + \Delta G_{ele,\,sol}$. (For interpretation of the references to color in this figure legend, the reader is referred to the web version of the article.)

which are nearly located on the surface of PKBα. These two residues do not have direct interaction with MK2206 or Lig1. Other hydrophilic residues, which have strong interactions with MK2206 or Lig1 as discussed above, have lower energy contributions to Lig2 binding to PKBα. (Gln79: -0.77 ± 0.02 kcal/mol, Thr82: -0.35 ± 0.02 kcal/mol, Ser205: 0.16 ± 0.02 kcal/mol, Tyr263: -1.03 ± 0.02 kcal/mol). Therefore, Lig2 has obviously weaker hydrophilic interactions with the binding pocket of PKBα than MK2206 or Lig1. These are supported by H-bond analyses (Table 1). It can be hypothesized that the residues Gln79, Thr82, and Ser205 in the binding pocket of PKB are important residues to have hydrophilic interactions with highly potent allosteric inhibitor since Lig2 do not have a corresponding H-bond acceptor or donor atom like MK2206 or Lig1.

Fig. 2c indicates that there are hydrophobic interactions between Lig2 and PKBα's hydrophobic residues. One of hydrophobic interactions is a stable π–π interaction happened between the pyridine ring A of Lig2 and the indole ring of Trp80. Comparing to MK2206 and Lig1, such a π–π interaction has a weaker energy contribution (-3.32 ± 0.02 kcal/mol) to Lig2 binding to PKBα since the pyridine ring A of Lig2 is obviously smaller than the aromatic fused ring A of either MK2206 or Lig1. The phenyl ring B linked on the C19 atom of Lig2 forms hydrophobic interactions with the phenyl groups of two residues of Tyr272 and Tyr263 since these aromatic rings are not parallel with each other. Per-residue energy decomposition calculation indicates that Tyr263 and Tyr272 provide more favorable hydrophobic interactions with MK2206 than Lig2. The energy contributions of Tyr263 and Tyr272 are -1.84 ± 0.02 kcal/mol and -2.54 ± 0.02 kcal/mol, respectively, to MK2206, but only -1.03 ± 0.01 kcal/mol and -0.18 ± 0.02 kcal/mol to Lig2. Although it is shown that Tyr263 provides a more favorable hydrophobic interaction with Lig2 (Tyr263: -1.03 ± 0.01 kcal/mol) than Lig1 (Tyr263: -0.52 ± 0.01 kcal/mol), other three hydrophobic residues Ile84 (Lig1: -2.64 ± 0.02 kcal/mol, Lig2: -1.04 ± 0.02 kcal/mol), Leu264 (Lig1: -2.33 ± 0.02 kcal/mol, Lig2: -1.99 ± 0.02 kcal/mol), and Tyr272 (Lig1: -0.45 ± 0.02 kcal/mol, Lig2: -0.18 ± 0.02 kcal/mol) provide more favorable hydrophobic interactions with Lig1 than Lig2. It can also be seen that the 5-substituted pyridine ring on the pyridine ring A of Lig2 can form a hydrophobic interaction with the butyl group of the side chain of Lys268. The phenyl ring C of Lig2 forms a hydrophobic interaction with Ile290. However, Lys268 (MK2206: -1.83 ± 0.02 kcal/mol, Lig1: -0.62 ± 0.02 kcal/mol, Lig2: -0.01 ± 0.02 kcal/mol), and Ile290

(MK2206: -0.87 ± 0.02 kcal/mol, Lig1: -0.69 ± 0.02 kcal/mol, Lig2: -0.60 ± 0.02 kcal/mol) provide more favorable hydrophobic interactions to MK2206 or Lig1 than Lig2. As shown in Fig. 6a, the residues Trp80, Tyr263, Lys268, Tyr272, and Ile290 of PKBα make more contributions of van der Waals and nonpolar solvation energies to MK2206 than Lig2. The residues Glu17, Gln79, Trp80, Thr81, Thr82, Glu85, Arg86, Val201, Leu264, Lys268, and Lys297 of PKBα make more contributions of van der Waals and nonpolar solvation energies to Lig1 than Lig2. Among these residues, Lys268 was validated to be important for the sensitivity to the inhibitor in the biochemical studies to replace the turn E267-K268-N269 in the kinase domain of PKBα by the residues Gly-Lys [64]. As illustrated in Fig. 6b, the total electrostatic energies of Gln79, Thr82, Ser205, and Tyr263 yield the energetic differences between MK2206 and Lig2. The total electrostatic energy of Ser205 yields the energetic difference between Lig1 and Lig2.

3.4. Proposal of a possible structural mechanism of PKBα's inhibition induced by allosteric inhibitor

Calleja et al. [39] proposed a model of MK2206 positioned in the PH Domain-induced cavity by 1 ns dynamic run. In the current studies, we performed a typical Steered molecular dynamics (SMD) simulations to predict a mechanism by which the inhibitor could enter deeply into the pocket formed by the PH and kinase domains of PKB when the protein is in the PH-in conformation was speculated (Supplementary data). As shown in Fig. S1, MK2206 was firstly anchored to PKB by the hydrogen bond interaction of the C-21 substituted primary amino group of MK2206 with the side chain carbonyl group of Glu114 when MK2206 was outside of the binding pocket. With the hydrophobic interaction of the phenyl ring C of MK2206 with the side chain of Val201, MK2206 moved toward the allosteric binding pocket. During the movements of MK2206 toward the gate of pocket, N7-H of MK2206 formed hydrogen bond interactions with the carbonyl groups of Asn204 and Ser205, while the N6 atom formed hydrogen bonds with the amino groups of Asn204, Ser205, and Lys268. Near the gate of the allosteric binding pocket, MK2206 was pulled into the pocket by the hydrophobic interactions of Trp80 with the phenyl ring C and the aromatic fused pyridine ring A of MK2206, respectively. In the binding pocket, MK2206 was stabilized by the hydrophobic interactions of MK2206 with the residues Trp80, Tyr263, and Leu264, and by the hydrogen bonds of MK2206 with the residues Tyr263 and Ser205. These above key interactions of MK2206 with PKBα were also confirmed by the inhibitor–residue interaction analysis of PKBα-MK2206 during the SMD run.

Biochemical data [39] have demonstrated that the allosteric inhibitors prevented the PDK1-catalyzed phosphorylation of Thr308 for the full activity of PKBα. Allosteric mode of PKBα inhibition is caused by the binding of allosteric inhibitors into the PH domain dependent pocket [2]. The allosteric inhibitor's binding is proposed to stabilize PKBα in a "closed" conformation in which PKBα is not capable of being phosphorylated at Thr308 promoted by PDK1. As shown in Fig. 7a, Thr308 is located in a flexible loop, which was defined as T-loop [65] of PKBα. T-loop is located near the allosteric pocket, which is surrounded by β6-strand, β7-strand, VL1 loop, and 1-loop of PH-domain, αE-helix, β1-strand, β2-strand, β8-strand, 2-loop, and 3-loop of the kinase domain. We superimposed the representative structure models of the three systems taken from last 2 ns MD trajectory. Fig. 7b illustrates different conformations of PKBα's T-loop, β6-strand, β7-strand, VL1 loop, 1-loop, αE-helix, β1-strand, β2-strand, β8-strand, 2-loop, and 3-loop in three complexes MK2206-PKBα, Lig1-PKBα, and Lig2-PKBα. Such conformational differences would be induced by variant interactions between different inhibitors and PKBα. In PKBα-MK2206, the 1-loop of PH-domain and T-loop of the kinase domain have significantly facing movements, which could be induced by the conformational changes of αE-helix including turn E267-K268-N269, during the MD simulation. The resulting conformation with the residues from 1-loop and T-loop near the activation loop theoretically may cause the steric hindrance for Thr308 phosphorylation showed by the experimental biochemical data [64].

For the prevention of Ser473 phosphorylation, our MD simulation results are in agreement with the biochemical data obtained by Calleja et al. [39,64]. In the present studies, we also supplied the coordinates of the C-terminus's missing residues Thr430-Ala480 in the X-ray co-crystal structure of PKBα-Lig1 (PDB entry: 3O96 [24]) according to the conformations of the corresponding C-terminal region in the crystal structures PKBα (PDB entry: 3MVH [44]) and PKBβ (PDB entry: 1O6K [45]) by aligning their kinase domains on the basis of homology method and performed 20 ns MD simulations. As shown in Fig. 7a for the MD-simulated complex PKBα-MK2206, the residue Gln218 is shown to be very close to Ser473. Ser473 and the C terminal domain are close to the allosteric binding site. The residue Gln218 are located in the vicinity of the allosteric binding site. The C terminal domain including Ser473 is close to residue Gln218 of the kinase domain. The side-chain amide group of Gln218 can form an H-bond with the backbone carbonyl group Ser473 within an interacting distance of 3.06 Å. These data can explain the biochemical data, reported by Calleja et al. [39,64], that the mutation of Gln218 can induce the loss of Ser473 phosphorylation. The distance between Gln218 and Thr308 is more than 25 Å, which is in accordance with that the mutation Q218A did not affect the Thr308 phosphorylation [39]. According to the structure of PKBα with MK2206 in Fig. 7a, Ser473 in C terminus is buried deeply at the interface between the PH and the kinase domains. It was thus speculated that the loss of Ser473 phosphorylation after allosteric inhibitor's binding could be likely caused by this steric hindrance to Ser473 interacting with mTORC2 complex and/or DNAPK [39].

Above all, the binding of the allosteric inhibitors not only induces the inactive kinase conformation to inhibit the phosphorylation of Thr308, but also stabilizes it by interacting with the residues Gln79, Trp80, Thr82, Glu85, Ser205, Tyr263, Tyr272, and Ile290 in the active pocket. All these results are congruent with the analyses of X-ray crystal structure of PKBα-Lig1 and the experimental bioactivities of the three inhibitors. The above illustration of the interactions between three allosteric inhibitors and PKBα here also provides pharmacophoric requirements for the development of novel PKBα allosteric inhibitors. Combining our MD simulation and binding free energy calculations of three allosteric inhibitors, with different inhibitory potencies, binding to PKBα and the related literatures [23,24,28,30,33,34,66], some clues could be proposed for the design of novel allosteric inhibitor with an improved efficacy based on the structure of MK2206. At first, the core ring A should be kept as an aromatic fused ring, which may have a parallel π–π interaction with the indole ring of the key residue Trp80. According to the results of our MD simulations, it is found that there should be a substituent with H-bond donor or acceptor, such as amino group or amide group, on the core ring A near the residue Ser205. This hydrophilic group may form an H-bond with the backbone peptide group of Ser205. Another substituent group, which is better to be a phenyl group, on the core ring A would be presented on the site of the ring C of MK2206 to have hydrophobic interactions with the residues Leu210, Ile290, and Tyr272. Since the amino group C21-NH_2 of MK2206 was illustrated as an H-bond acceptor to have H-bond interactions with the residues Gln79 and Thr82, an H-bond acceptor would be designed at the corresponding point. In addition, the part D of Lig2 should be erased to decrease molecular weight since our MD simulations indicated that this part of Lig2 did not have significant interaction with the residues around the binding pocket of PKBα for its allosteric inhibitor.

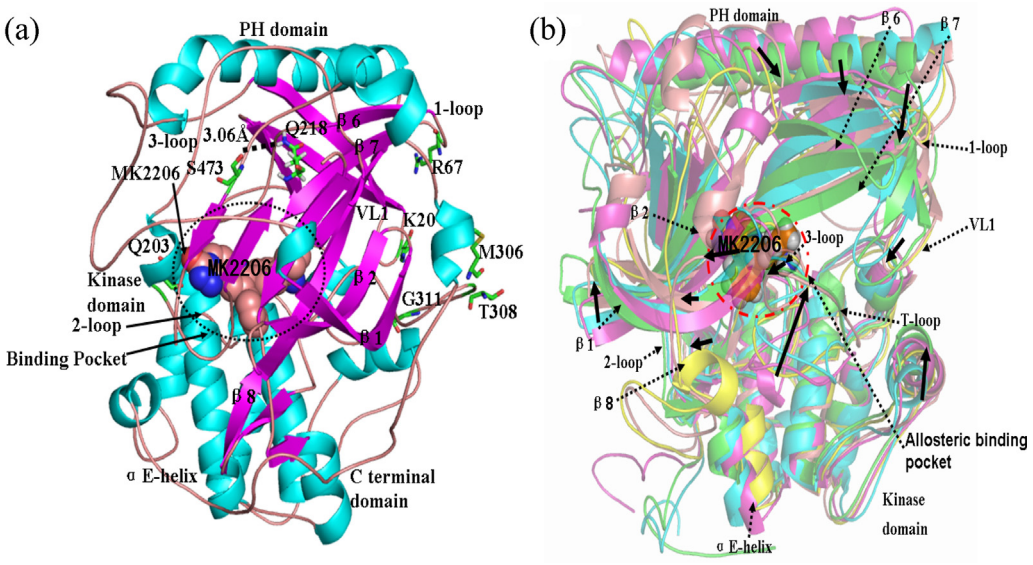

Fig. 7. (a) Representative snapshot of the complex of PKBα-MK2206 from the MD results. (PKBα in colored ribbon, MK2206 in CPK model, the key residues in sticks model.) (b) Structure comparison of representative snapshots from 20 ns MD of PKBα-MK2206 (green), PKBα-Lig1 (cyan), PKBα-Lig2 (pink) and the initial structural model of PKBα-MK2206 (yellow). The black arrows represent the directions of the changes of the complexes.

4. Conclusions

In the current study, MD simulations and free energy calculations were executed to investigate the structural mechanisms of three allosteric inhibitors MK2206, Lig1, and Lig2, respectively, binding to PKBα. The per-residue energy decomposition was also performed to demonstrate the favorable and unfavorable interactions of individual residue with inhibitor. Our results indicated that the computed binding free energies of these three inhibitors were congruent with the ranking of their experimental IC_{50} values. The analyses of the components in binding free energy suggested that the major contributions to inhibitors binding to PKBα were the van der Waals energy components of Trp80, Tyr263, Lys268, Tyr272, and Ile290. The inhibitors can only have the bioactivity when they contain the suitable aromatic fused ring and substituents to form the hydrophobic interactions with the corresponding residues. In addition, these van der Waals interactions also stabilize the "PH-in" conformation of PKBα. On the other hand, the highly potent allosteric inhibitor would have essential H-bond acceptor or donor to interact with the hydrophilic residues Gln79, Thr82, Ser205, and Tyr263 of PKBα. The studies proposed the potential pharmacophoric requirements for bioactive allosteric inhibitor binding to PKBα. That would be useful chemical or biochemical informatics for the design of new allosteric inhibitors.

Acknowledgment

The authors are thankful to the College of Pharmaceutical Sciences, Zhejiang University for providing necessary facilities.

Appendix A. Supplementary data

Supplementary data associated with this article can be found, in the online version, at http://dx.doi.org/10.1016/j.jmgm.2013.12.002.

References

[1] S.F. Barnett, M.T. Bilodeau, C.W. Lindsley, The Akt/PKB family of protein kinases: a review of small molecule inhibitors and progress towards target validation, Curr. Top. Med. 5 (2005) 109–125.
[2] C.W. Lindsley, S.F. Barnett, M. Yaroschak, M.T. Bilodeau, M.E. Layton, Recent progress in the development of ATP-competitive and allosteric Akt kinase inhibitors, Curr. Top. Med. 7 (2007) 1349–1363.
[3] G.Z. Cheng, S. Park, S. Shu, L. He, W. Kong, W. Zhang, et al., Advances of AKT pathway in human oncogenesis and as a target for anti-cancer drug discovery, Curr. Cancer Drug Target. 8 (2008) 2–6.
[4] E. Fayard, L.A. Tintignac, A. Baudry, B.A. Hemmings, Protein kinase B/Akt at a glance, J. Cell Sci. 118 (2005) 5675–5678.
[5] I. Collins, Targeted small-molecule inhibitors of protein kinase B as anticancer agents, Anticancer Agents Med. Chem. 9 (2009) 32–50.
[6] Q. Li, G.D. Zhu, Targeting serine/threonine protein kinase B/Akt and cell-cycle checkpoint kinases for treating cancer, Curr. Top. Med. 2 (2002) 939–971.
[7] M. Mizoguchi, C.L. Nutt, G. Mohapatra, D.N. Louis, Genetic alterations of phosphoinositide 3-kinase subunit genes in human glioblastomas, Brain Pathol. 14 (2004) 372–377.
[8] L. Shayesteh, Y. Lu, W.L. Kuo, R. Baldocchi, T. Godfrey, C. Collins, et al., PIK3CA is implicated as an oncogene in ovarian cancer, Nat. Genet. 21 (1999) 99–102.
[9] D.S. Byun, K. Cho, B.K. Ryu, M.G. Lee, J.I. Park, K.S. Chae, et al., Frequent monoallelic deletion of PTEN and its reciprocal associatioin with PIK3CA amplification in gastric carcinoma, Int. J. Cancer 104 (2003) 318–327.
[10] J.M. Pedrero, D.G. Carracedo, C.M. Pinto, A.H. Zapatero, J.P. Rodrigo, C.S. Nieto, et al., Frequent genetic and biochemical alterations of the PI3-K/AKT/PTEN pathway in head and neck squamous cell carcinoma, Int. J. Cancer 114 (2005) 242–248.
[11] B.I. Bertelsen, S.J. Steine, R. Sandvei, A. Molven, O.D. Laerum, Molecular analysis of the PI3K–AKT pathway in uterine cervical neoplasia: frequent PIK3CA amplification and AKT phosphorylation, Int. J. Cancer 118 (2006) 1877–1883.
[12] I. Sansal, W.R. Sellers, The biology and clinical relevance of the PTEN tumor suppressor pathway, J. Clin. Oncol. 22 (2004) 2954–2963.
[13] S. Faivre, G. Kroemer, E. Raymond, Current development of mTOR inhibitors as anticancer agents, Nat. Rev. Drug Discov. 5 (2006) 671–688.
[14] B.T. Hennessy, D.L. Smith, P.T. Ram, Y. Lu, G.B. Mills, Exploiting the PI3K/AKT pathway for cancer drug discovery, Nat. Rev. Drug Discov. 4 (2005) 988–1004.
[15] A. Bellacosa, D. de Feo, A.K. Godwin, D.W. Bell, J.Q. Cheng, D.A. Altomare, et al., Molecular alterations of the AKT2 oncogene in ovarian and breast carcinomas, Int. J. Cancer 64 (1995) 280–285.
[16] K. Nakayama, N. Nakayama, R.J. Kurman, L. Cope, G. Pohl, Y. Samuels, et al., Sequence mutations and amplification of PIK3CA and AKT2 genes in purified ovarian serous neoplasms, Cancer Biol. Ther. 5 (2006) 779–785.
[17] B.A. Ruggeri, L. Huang, M. Wood, J.Q. Cheng, J.R. Testa, Amplification and overexpression of the AKT2 oncogene in a subset of human pancreatic ductal adenocarcinomas, Mol. Carcinogen. 21 (1998) 81–86.
[18] W. Miwa, J. Yasuda, Y. Murakami, K. Yashima, K. Sugano, T. Sekine, et al., Isolation of DNA sequences amplified at chromosome 19q13.1–q13.2 including the AKT2 locus in human pancreatic cancer, Biochem. Bioph. Res. Commun. 225 (1996) 968–974.
[19] H.K. Roy, B.F. Olusola, D.L. Clemens, W.J. Karolski, A. Ratashak, H.T. Lynch, et al., AKT proto-oncogene overexpression is an early event during sporadic colon carcinogenesis, Carcinogenesis 23 (2002) 201–205.
[20] Y.L. Chen, P.Y. Law, H.H. Loh, Inhibition of PI3K/Akt signaling: an emerging paradigm for targeted cancer therapy, Curr. Med. Chem. Anti-Cancer Agents 5 (2005) 575–589.

[21] S.F. Barnett, D.D. Jones, S. Fu, P.J. Hancock, K.M. Haskell, R.E. Jones, et al., Identification and characterization of pleckstrin-homology-domain dependent and isoenzyme-specific Akt inhibitors, Biochem. J. 385 (2005) 399–408.
[22] H. Hirai, H. Sootome, Y. Nakatsuru, K. Miyama, S. Taguchi, K. Tsujioka, et al., MK-2206, an allosteric akt inhibitor, enhances antitumor efficacy by standard chemotherapeutic agents or molecular targeted drugs in vitro and in vivo, Mol. Cancer Ther. 9 (2010) 1956–1967.
[23] Z. Zhao, W.H. Leister, R.G. Robinson, S.F. Barnett, D.D. Jones, R.E. Jones, et al., Discovery of 2,3,5-trisubstituted pyridine derivatives as potent Akt1 and Akt2 dual inhibitors, Bioorg. Med. Chem. Lett. 15 (2005) 905–909.
[24] W.I. Wu, W.C. Voegtli, H.L. Sturgis, F.P. Dizon, G.P.A. Vigers, B.J. Brandhuber, Crystal structure of human AKT1 with an allosteric inhibitor reveals a new mode of kinase inhibition, PLoS ONE 5 (2010) 1–9.
[25] J.C. Hartnett, S.F. Barnett, M.T. Bilodeau, D. Defeo-Jones, G.D. Hartman, H.E. Huber, et al., Optimization of 2,3,5-trisubstituted pyridine derivatives as potent allosteric Akt1 and Akt2 inhibitors, Bioorg. Med. Chem. Lett. 18 (2008) 2194–2197.
[26] C.W. Lindsley, Z. Zhao, W.H. Leister, R.G. Robinson, S.F. Barnett, D. Defeo-Jones, et al., Allosteric Akt (PKB) inhibitors: discovery and SAR of isozyme selective inhibitors, Bioorg. Med. Chem. Lett. 15 (2005) 761–764.
[27] L.T. Barza, W.G. Zhang, X.Y. Huang, L.A. McDonald, E.J. Salaski, L.R. Barbieri, et al., Discovery of lactoquinomycin and related pyranonaphthoquinones as potent and allosteric inhibitors of AKT/PKB: mechanistic involvement of AKT catalytic activation loop cysteines, Mol. Cancer Ther. 6 (2007) 3028–3038.
[28] M.T. Bilodeau, A.E. Balitza, J.M. Hoffman, P.J. Manley, S.F. Barnett, D. Defeo-Jones, et al., Allosteric inhibitors of Akt1 and Akt2: a naphthyridinone with efficacy in an A2780 tumor xenograft model, Bioorg. Med. Chem. Lett. 18 (2008) 3178–3182.
[29] C.W. Lindsley, S.F. Barnett, M.E. Layton, M.T. Bilodeau, The PI3K/Akt pathway: recent progress in the development of atp-competitive and allosteric Akt kinase inhibitors, Curr. Cancer Drug Target. 8 (2008) 7–18.
[30] T. Siu, Y. Li, J. Nagasawa, J. Liang, L. Tehrani, P. Chua, et al., The design and synthesis of potent and cell-active allosteric dual Akt 1 and 2 inhibitors devoid of hERG activity, Bioorg. Med. Chem. Lett. 18 (2008) 4191–4194.
[31] T. Siu, J. Liang, J. Arruda, Y. Li, R.E. Jones, D. Defeo-Jones, et al., Discovery of potent and cell-active allosteric dual Akt 1 and 2 inhibitors, Bioorg. Med. Chem. Lett. 18 (2008) 4186–4190.
[32] Z. Wu, R.G. Robinson, S. Fu, S.F. Barnett, D. Defeo-Jones, R.E. Jones, et al., Rapid assembly of diverse and potent allosteric Akt inhibitors, Bioorg. Med. Chem. Lett. 18 (2008) 2211–2214.
[33] Z. Zhao, R.G. Robinson, S.F. Barnett, D. Defeo-Jones, R.E. Jones, G.D. Hartman, et al., Development of potent, allosteric dual Akt1 and Akt2 inhibitors with improved physical properties and cell activity, Bioorg. Med. Chem. Lett. 18 (2008) 49–53.
[34] Y. Li, J. Liang, T. Siu, E. Hu, M.A. Rossi, S.F. Barnett, et al., Allosteric inhibitors of Akt1 and Akt2: discovery of [1,2,4]triazolo[3,4-*f*][1,6]naphthyridines with potent and balanced activity, Bioorg. Med. Chem. Lett. 19 (2009) 834–836.
[35] J. Yun, Allosteric AKT inhibitors as a targeted cancer therapy, Cancer Biol. Ther. 9 (2010) 504–506.
[36] J.G. Kettle, S. Brown, C. Crafter, B.R. Davies, P. Dudley, G. Fairley, et al., Diverse heterocyclic scaffolds as allosteric inhibitors of AKT, J. Med. Chem. 55 (2011) 1261–1273.
[37] K.D. Joon, K. Reddy, M.O. Kim, Y. Li, J. Nadas, Y.Y. Cho, et al., (3-Chloroacetyl)-indole, a novel allosteric AKT inhibitor suppresses colon cancer growth in vitro and in vivo, Cancer Prev. Res. 4 (2011) 1842–1851.
[38] Y. Yang, Y. Shen, H. Liu, X. Yao, Molecular dynamics simulation and free energy calculation studies of the binding mechanism of allosteric inhibitors with p38α MAP kinase, J. Chem. Inf. Model. 51 (2011) 3235–3246.
[39] V. Calleja, M. Laguerre, P.J. Parker, B. Larijani, Role of a novel PH-kinase domain interface in PKB/Akt regulation: structural mechanism for allosteric inhibition, PLoS Biol. 7 (2009) 189–200.
[40] N.M. Mascarenhas, D. Bhattacharyya, N. Ghoshal, Why pyridine containing pyrido[2,3-*d*]pyrimidin-7-ones selectively inhibit CDK4 than CDK2: insights from molecular dynamics simulation, J. Mol. Graph. Model. 28 (2010) 695–706.
[41] Q. Chen, W. Cui, Y. Cheng, F. Zhang, M. Ji, Studying the mechanism that enables paullones to selectively inhibit glycogen synthase kinase 3 rather than cyclin-dependent kinase 5 by molecular dynamics simulations and free-energy calculations, J. Mol. Model. 17 (2011) 795–803.
[42] P.A. Kollman, I. Massova, C. Reyes, B. Kuhn, S. Huo, L. Chong, et al., Calculating structures and free energies of complex molecules: combining molecular mechanics and continuum models, Acc. Chem. Res. 33 (2000) 889–897.
[43] H. Gohlke, C. Kiel, D.A. Case, Insights into protein–protein binding by binding free energy calculation and free energy decomposition for the Ras-Raf and Ras-RalGDS complexes, J. Mol. Biol. 330 (2003) 891–913.
[44] K.D. Freeman-Cook, C. Autry, G. Borzillo, D. Gordon, E. Barbacci-Tobin, V. Bernardo, et al., Design of selective, ATP-competitive inhibitors of Akt, J. Med. Chem. 53 (2010) 4615–4622.
[45] J. Yang, P. Cron, V.M. Good, V. Thompson, B.A. Hemmings, D. Barford, Crystal structure of an activated Akt/Protein Kinase B ternary complex with GSK3-peptide and AMP-PNP, Nat. Struct. Biol. 9 (2002) 940–944.
[46] SYBYL-X 1.3, T.I., 1699 South Hanley Rd., St. Louis, MI 63144, USA.
[47] D.A. Case, T.A. Darden, T.E. Cheatham, C.L. Simmerling, J. Wang, R.E. Duke, et al., AMBER 11, University of California, San Francisco, 2010.
[48] V. Tsui, D.A. Case, Theory and applications of the generalized Born solvation model in macromolecular simulations, Biopolymers 56 (2001) 275–291.
[49] Y. Duan, C. Wu, S. Chowdhury, M.C. Lee, G. Xiong, W. Zhang, et al., A point-charge force field for molecular mechanics simulations of proteins based on condensed-phase quantum mechanical calculations, J. Comput. Chem. 24 (2003) 1999–2012.
[50] J. Wang, R.M. Wolf, J.W. Caldwell, P.A. Kollman, D.A. Case, Development and testing of a general amber force field, J. Comput. Chem. 25 (2004) 1157–1174.
[51] T. Darden, D. York, L. Pedersen, Particle mesh Ewald: an $N \log(N)$ method for Ewald sums in large systems, J. Chem. Phys. 98 (1993) 10089–10092.
[52] J.P. Ryckaert, G. Ciccotti, H.J.C. Berendsen, Numerical integration of the cartesian equations of motion of a system with constraints: molecular dynamics of n-alkanes, J. Comput. Phys. 23 (1977) 327–341.
[53] H.J.C. Berendsen, J.P.M. Postma, Gunsteren W.F.V., A. DiNola, J.R. Haak, Molecular dynamics with coupling to an external bath, J. Chem. Phys. 81 (1984) 3684–3690.
[54] W. Rocchia, E. Alexov, B. Honig, Extending the applicability of the nonlinear Poisson–Boltzmann equation: multiple dielectric constants and multivalent ions, J. Phys. Chem. B 105 (2001) 6507–6514.
[55] A. Onufriev, D. Bashford, D.A. Case, Exploring protein native states and large-scale conformational changes with a modified generalized born model, Proteins: Struct. Funct. Bioinform. 55 (2004) 383–394.
[56] J. Weiser, P.S. Shenkin, W.C. Still, Approximate atomic surfaces from linear combinations of pairwise overlaps (LCPO), J. Comput. Chem. 20 (1999) 217–230.
[57] M.L. Connolly, Analytical molecular-surface calculation, J. Appl. Crystallogr. 16 (1983) 548–558.
[58] C. Tan, Y.H. Tan, R. Luo, Implicit nonpolar solvent models, J. Phys. Chem. B 111 (2007) 12263–12274.
[59] M. Pinto, M.d.M. Orzaez, L.D. Soler, J.J. Perez, J.R. Martinez, Rational design of new class of BH3-mimetics as inhibitors of the Bcl-x_L protein, J. Chem. Inf. Model. 51 (2011) 1249–1258.
[60] C.I. Bayly, P. Cieplak, W.D. Cornell, P.A. Kollman, A well-behaved electrostatic potential based method using charge restraints for deriving atomic charges: the RESP model, J. Phys. Chem. 97 (1993) 10269–10280.
[61] R.C. Rizzo, J.T. Rives, W.L. Jorgensen, Estimation of binding affinities for HEPT and nevirapine analogues with HIV-1 reverse transcriptase via Monte Carlo simulations, J. Med. Chem. 44 (2001) 145–154.
[62] B. Aguilar, A. Onufriev, Efficient computation of the total solvation energy of small molecules via the R6 generalized born model, J. Chem. Theory Comput. 8 (2012) 2404–2411.
[63] H. Gohlke, C. Kiel, D.A. Case, Insights into protein–protein binding by binding free energy calculation and free energy decomposition for the Ras-Raf and Ras-RalGDS complexes, J. Mol. Biol. 330 (2003) 891–913.
[64] V. Calleja, M. Laguerre, B. Larijani, Role of the C-terminal regulatory domain in the allosteric inhibition of PKB/Akt, Adv. Enzyme Regul. 52 (2012) 46–57.
[65] M.P. Schael, J.R. Woodgett, PKB/Akt: functional insights from genetic models, Nat. Rev. Mol. Cell Biol. 2 (2001) 760–768.
[66] C.W. Lindsley, M.J. Bogusky, W.H. Leister, R.T. McClain, R.G. Robinson, S.F. Barnett, et al., Synthesis and biological evaluation of unnatural canthine alkaloids, Tetrahedron Lett. 46 (2005) 2779–2782.